2015 IEEE/RSJ International Conference on Intelligent Robots and Systems (IROS)
Congress Center Hamburg
Sept 28 - Oct 2, 2015. Hamburg, Germany

Information-Theoretic Occupancy Grid Compression for High-Speed Information-Based Exploration

Erik Nelson and Nathan Michael

Abstract— **We propose information-theoretic strategies for Occupancy Grid (OG) compression to enable high-speed exploration on computationally constrained mobile robots. We first formulate optimal lossy compression for OGs based on the Principle of Relevant Information. The solution to this formulation is a simple compression algorithm that is motivated by rate distortion theory. We then compress OGs to different resolutions and develop a second optimization based on the Information Bottleneck method that chooses a resolution simultaneously maximizing compression and minimizing loss of information from the robot's sensor measurements. On computationally constrained systems, the resulting reduction in computational complexity enables planning over longer predictive horizons, leading to higher-speed operation. Using these techniques to adaptively optimize OG resolution as the robot enters a new area causes it to autonomously slow down in obstacle-dense locations and speed up in open expanses. We simulate and experimentally evaluate mutual information-based exploration through cluttered indoor environments with exploration rates that adapt based on environment complexity, leading to an order-of-magnitude increase in the maximum rate of exploration in contrast to non-adaptive techniques given the same finite computational resources.**

I. Introduction

In this paper, we propose map compression methods to reduce the computational burden associated with autonomous mobile robot exploration strategies. Recent exploration methods employ techniques that reduce map uncertainty by choosing control actions that optimize information-theoretic metrics [1, 2, 7]. While these solutions yield increased exploration performance [4], in contrast to techniques that reason about the geometry of unknown space in the map [3, 17, 20], information-based strategies are more computationally expensive, possessing a computational complexity that scales linearly with the map's resolution. Therefore, we propose a technique that seeks to reduce the computational complexity through lossy map compression while only minimally degrading exploration performance. On computationally constrained systems, the resulting reduction in complexity enables planning over longer predictive horizons, leading to higher-speed operation.

The proposed map compression strategy leverages techniques from rate-distortion theory and signal processing that reduce a random variable to a compressed form while minimizing distortion between the original and reduced representations. Specifically, we consider Occupancy Grid (OG) maps [6] and develop a formulation for compressing an OG to a specified grid cell resolution that minimizes information loss about sensor measurements using the Principle of Relevant Information (PRI) [15] and Information Bottleneck (IB) method [19].

Several map compression strategies are proposed in the literature. The OctoMap framework [9] builds an octree data structure to efficiently store the expected occupancy of cells in an environment without allocating memory for a large 3D grid. Im et al. [10] compress an OG by representing it with wavelets using the Haar wavelet transform. Kretzschmar and Stachniss [12] compress pose graph maps by examining the Shannon mutual information between the pose graph and sensor measurements. Most related to the proposed technique, Einhorn et al. [5] adaptively choose an OG resolution for individual cells by determining which cells are intersected by measurements. In contrast to these works, we approach the map compression problem as one of simultaneously reducing the distortion between the map and its compressed form, and between a compressed map and sensor measurements.

Information-based exploration methods generally choose control actions that seek to maximize the informativeness of future sensor observations, yielding a reduction in map uncertainty computed via metrics such as Shannon mutual information (MI) [1, 2, 7, 11] and Cauchy-Schwarz quadratic mutual information (CSQMI) [4]. Similar to the work of Charrow et al. [4], we choose to employ CSQMI due to the favorable analytic properties and increased computational efficiency.

An outline of the methodology presentation follows. We first provide an overview of OG mapping and the CSQMI reward metric (Sect. II). Section III develops a simple rule for compressing an OG to a specified resolution using the PRI, and provides an IB-based strategy for determining an OG resolution that maximizes compression and minimizes loss of information about a sensor measurement. Section III-C describes a technique to adapt the OG resolution whenever the complexity of its local map changes, and Sect. IV overviews a receding horizon planner used to generate candidate exploration actions. Results in both simulation and on a ground robot demonstrate that compressing an OG dramatically increases the efficiency of computing CSQMI, thereby allowing the robot to plan faster and move at higher velocities (Sect. V).

The authors are members of the Robotics Institute, Carnegie Mellon University, 5000 Forbes Avenue, Pittsburgh, PA 15213. Email: {enelson,nmichael}@cmu.edu

We gratefully acknowledge the support of ARL grant W911NF-08-2-0004.

II. Environment Model

We represent the map as an OG, which decomposes the robot's workspace into a discrete set of cells. The presence or absence of obstacles within these cells is modeled as a K-tuple binary random variable, $m = \{m_i\}_{i=1}^{K}$, with support set $\{\texttt{EMP}, \texttt{OCC}\}$. The probability that an individual cell is occupied is given by $p(m_i \mid x_{1:t}, z_{1:t})$, where $x_{1:t}$ denotes the history of states of the vehicle, and $z_{1:t}$ denotes the history of range observations accumulated by the vehicle. The OG representation treats cells as independent from one another, allowing one to express the probability of a specific map as the product of individual cell occupancy values: $p(m \mid x_{1:t}, z_{1:t}) = \prod_i p(m_i \mid x_{1:t}, z_{1:t})$. For notational simplicity we write the map conditioned on random variables $x_{1:t}$ and $z_{1:t}$ as $p(m) \equiv p(m \mid x_{1:t}, z_{1:t})$, and the probability of occupancy for a grid cell i as $o_i \equiv p(m_i = \texttt{OCC})$. Unobserved grid cells are assigned a uniform prior such that $\{o_i = 1 - o_i = 0.5\}_{i=1}^{K}$. To allow cell occupancy values to be updated with new measurements, we represent the occupancy status of grid cell m_i at time t with the log-odds expression

$$l_t \equiv \log \frac{o_i}{1 - o_i}.$$

When a new measurement z_t is obtained, cell occupancy values may be updated with

$$l_t = l_{t-1} + L(m_i \,|z_t),$$

where the term $L(m_i \,|z_t)$ represents the robot's inverse sensor model [18].

A. CSQMI as an Exploration Reward Metric

Following Charrow et al. [4], we formulate an exploration control policy by choosing actions that maximize the Cauchy-Schwarz quadratic mutual information (CSQMI) between the robot's expected future sensor measurements and its current map. We define an action as a sequence of poses $x_\tau \equiv (x_i)_{i=t+1}^{t+T}$ navigated during a future time interval $\tau \equiv (t+1, \ldots, t+T)$. From poses x_τ, the robot will acquire future sensor measurements $z_\tau \equiv (z_i(x_i))_{i=t+1}^{t+T}$. In practice, actions are selected from a library of motion primitives $\mathcal{X}_\tau$ generated by a planner (Sect. IV). Therefore, the most informative action is the one that maximizes information:

$$x_\tau^* = \underset{x_\tau \in \mathcal{X}_\tau}{\operatorname{argmax}} \; \mathrm{I_{CS}}(m; z_\tau(x_\tau)), \tag{1}$$

where $\mathrm{I_{CS}}(m; z_\tau(x_\tau)) \in \mathbb{R}_+$ is the CSQMI between the robot's map and expected future measurements:

$$\mathrm{I_{CS}}(m; z_\tau) = \log \frac{\int \sum_m p^2(m) p^2(z_\tau)\, dz_\tau \int \sum_m p^2(m,\, z_\tau)\, dz_\tau}{\left(\int \sum_m p(m,\, z_\tau)\, p(m)\, p(z_\tau)\, dz_\tau\right)^2}. \tag{2}$$

We use CSQMI as it can be computed exactly in $\mathcal{O}(n^2)$, and to a close approximation in $\mathcal{O}(n)$, where n is the number of grid cells intersected by z_τ. CSQMI is closely related to the more common Shannon mutual information (MI). Both metrics describe a distance between probability distributions $p(m, z_\tau)$ and $p(m)\, p(z_\tau)$. To see that CSQMI describes this distance, note that Eq. (2) is non-negative and is equal to zero if and only if m and z_τ are independent. Importantly, CSQMI and MI are similar when evaluated on an OG with a beam-based sensor model, and control actions that maximize CSQMI guide the robot to unexplored space (Fig. 1). For discussion regarding the calculation of CSQMI, we refer the reader to work of Charrow et al. [4].

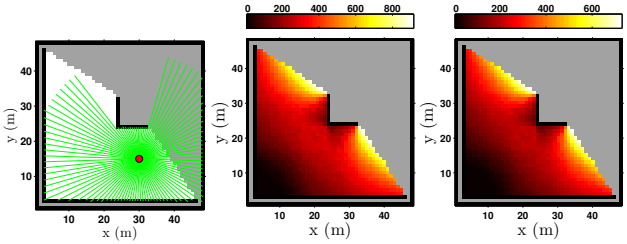

(a) Map and sample measurement (b) MI (c) CSQMI

Fig. 1: MI (1b) and CSQMI (1c) densely computed in free space over an occupancy grid (1a) using a 100-beam omnidirectional 2D laser with 30 m range.

III. Information-Theoretic Occupancy Grid Compression

In this section, we describe an information-theoretic strategy for compressing an OG to a specified resolution using the Principle of Relevant Information [15]. We then develop a second optimization based on the Information Bottleneck method [19] to determine the grid resolution that maximizes compression and minimizes loss of mutual information with respect to expected future sensor measurements. The motivation for OG compression originates from the fact that the complexity of computing CSQMI between an OG and a beam-based measurement scales linearly (using the approximate technique introduced by Charrow et al. [4]) with the number of cells intersected by the measurement (Fig. 2). Exploiting this fact by compressing the OG to a lower resolution can lead to significant computational efficiency gains. However, OG compression results in distortion to the map and to information-based reward; after too much compression, the optimization in Eq. (1) will select suboptimal actions. The goal of the following section is to develop strategies for balancing compression (efficiency) with fidelity of information (accuracy) about the robot's measurements.

A. Principle of Relevant Information

OG compression can be formulated as an information-theoretic optimization using the Principle of Relevant Information (PRI). PRI is a technique for learning a reduced representation $\hat{X}$ of a random variable X such that both the entropy of $\hat{X}$ and the divergence of $\hat{X}$ with respect to the original data are minimized:

$$J(\hat{X}) = \min_{\hat{X}} (\mathrm{H}_\alpha(\hat{X}) + \lambda \mathrm{D}_\alpha(X || \hat{X})). \tag{3}$$

The two terms of the PRI cost function are Rényi's α-entropy, which describes the amount of uncertainty in its

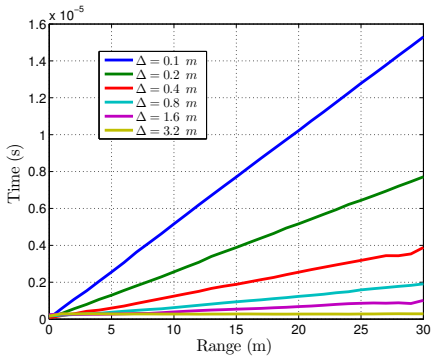

Fig. 2: Time (median of 10^5 samples) to evaluate CSQMI for a single beam is linear in both the OG resolution Δ, and the measurement range.

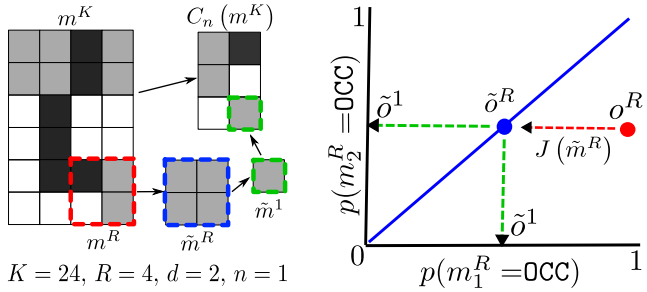

(a) OG compression sequence

(b) Probability space of the top two grid cells in m^R in 3a

Fig. 3: For each square (cubic in 3D) region m^R in the uncompressed OG m^K, the PRI optimization finds a random variable $\tilde{m}^R$ that minimizes Eq. (3) and is constrained to have uniform occupancy probability $\tilde{o}^R = (\tilde{o}^1, \ldots, \tilde{o}^1)$.

argument, and Rényi's α-divergence, a distance measure describing distortion between $p(x)$ and $p(\hat{x})$. These terms simplify to the more common Shannon entropy and Kullback-Leibler divergence for $\alpha = 1$. The variational parameter λ controls the amount of distortion in the compressed data. To complement the Information Bottleneck optimization described later (Sect. III-B), we choose to minimize the H_2 entropy and Cauchy-Schwarz divergence. For discrete random variables X and $\hat{X}$,

$$\mathrm{H}_2(\hat{X}) = -\log \sum_i p^2(\hat{x}_i), \tag{4}$$

$$\mathrm{D}_{\mathrm{CS}}(X||\hat{X}) = \log \frac{\sum_i p^2(x_i) \sum_i p^2(\hat{x}_i)}{\left(\sum_i p(x_i)p(\hat{x}_i)\right)^2}. \tag{5}$$

The cost function in Eq. (3) is then:

$$(1-\lambda)\,\mathrm{H}_2(\hat{X}) - \lambda 2 \log \sum_i p(x_i)p(\hat{x}_i) - \lambda \mathrm{H}_2(X). \tag{6}$$

The third term has no influence on the minimization over $\hat{X}$, and can be ignored. We choose to give equal weight to the entropy and divergence, and optimize for $\lambda = 1$. Noting that logs and quadratic functions increase monotonically for positive arguments, and noting that the summand in the second term of Eq. (6) must be positive, the optimization can be simplified to:

$$J(\hat{X}) = \max_{\hat{X}} \sum_i p(x_i)p(\hat{x}_i). \tag{7}$$

To apply the PRI optimization to OG compression, let X be an OG m^K with K cells. The problem must be constrained in three ways. First, as OGs encode a 2D or 3D geometry, $\hat{X}$ must represent X well in local regions. Compression over the map can therefore be accomplished by performing compression in many small independent square (cubic in 3D) regions $m^R \subseteq m^K$, assuming individual grid cell occupancies are independent. Second, we consider only the set of compressions that reduce OG cell count in each dimension by factors of two. Therefore an OG m^K will be compressed to an OG $m^{2^{-dn}K}$, where d is the number of OG dimensions and n is the number of $2\times$ compressions in each dimension. The set of compressions with this property can be expressed as:

$$C_n(m^K) \equiv m^{2^{-dn}K}, \quad n \in \mathbb{N}_0,$$

where superscripts denote cell count and where a compression of $n = 0$ gives the original OG: $C_0(m^K) = m^K$. Both m^K and $C_n(m^K)$ will have the same metric dimensions, but will have different cell edge lengths and cell counts when $n \geq 1$. Finally, we enforce that $\hat{X}$ must also be an OG. Since $\mathrm{D}_{\mathrm{CS}}(X||\hat{X})$ may only be computed for two random variables with the same support set, we use the PRI to find a random variable $\tilde{m}^R$ that has uniform occupancy probabilities, and then reduce its dimension to one, yielding a single grid cell $\tilde{m}^1$ (Fig. 3). Combining the single-cell $\tilde{m}^1$ variables from independent regions yields the compressed OG $C_n(m^K)$.

Rather than directly maximizing Eq. (7) over $\tilde{m}^R$, we are interested in finding the distribution $p(\tilde{m}^R)$ corresponding to the maximum. $p(\tilde{m}^R)$ is a Bernoulli distribution, and is completely determined by its single parameter $\tilde{o}^1 = p(\tilde{m}^R = \{\texttt{OCC}, \ldots, \texttt{OCC}\}) = 1 - p(\tilde{m}^R = \{\texttt{EMP}, \ldots, \texttt{EMP}\})$. Substituting the described variables into Eq. (7),

$$\tilde{o}^1_* = \operatorname*{argmax}_{\tilde{o}^1} \sum_{\substack{\{\{\texttt{OCC},\ldots,\texttt{OCC}\},\\ \{\texttt{EMP},\ldots,\texttt{EMP}\}\}}} p\left(m^R\right) p\left(\tilde{m}^R\right). \tag{8}$$

Table I is a contingency table for a compression from the OG region m^R to $\tilde{m}^R$. The middle columns of the contingency table have zero probability, since $\tilde{m}^R$ must have a uniform cell probability in order for it to be reduced to $\tilde{m}^1$ (i.e. $\tilde{o}^R_i = \tilde{o}^R_j = \tilde{o}^1,\ \forall i,j \in \{1,\ldots,R\}$). In this section, we are only interested in the marginal distributions (bottom-most row and right-most column), which are needed to determine Eq. (8). Substituting these values:

$$\tilde{o}^1_* = \operatorname*{argmax}_{\tilde{o}^1} \left((1-\tilde{o}^1) \prod_{i=1}^{R} (1 - o_i^R) + \tilde{o}^1 \prod_{i=1}^{R} o_i^R \right),$$

which is satisfied for

$$\tilde{o}^1_* = \begin{cases} 0 & \text{if } \prod_{i=1}^R \frac{o_i^R}{1-o_i^R} < 1 \\ 1 & \text{if } \prod_{i=1}^R \frac{o_i^R}{1-o_i^R} > 1 \\ \frac{1}{2} & \text{otherwise} \end{cases}, \tag{9}$$

TABLE I: Contingency table for a compression from the OG region m^R to $\tilde{m}^R$. O and E stand for OCC and EMP.

		$\tilde{m}^R$					
		E, E, …, E	E, E, …, O	…	O, O, …, E	O, O, …, O	Total
m^R	E, E, …, E	$\prod_{i=1}^{R}(1-o_i^R)\cdot p(\tilde{m}^R \mid m^R)$	0	…	0	$\prod_{i=1}^{R}(1-o_i^R)\cdot p(\tilde{m}^R \mid m^R)$	$\prod_{i=1}^{R}(1-o_i^R)$
	E, E, …, O	$o_1^R\cdot\prod_{i=2}^{R}(1-o_i^R)\cdot p(\tilde{m}^R \mid m^R)$	0	…	0	$o_1^R\cdot\prod_{i=2}^{R}(1-o_i^R)\cdot p(\tilde{m}^R \mid m^R)$	$o_1^R\cdot\prod_{i=2}^{R}(1-o_i^R)$
	⋮	⋮	⋮	⋱	⋮	⋮	⋮
	O, O, …, E	$(1-o_1^R)\cdot\prod_{i=2}^{R}o_i^R\cdot p(\tilde{m}^R \mid m^R)$	0	…	0	$(1-o_1^R)\cdot\prod_{i=2}^{R}o_i^R\cdot p(\tilde{m}^R \mid m^R)$	$(1-o_1^R)\cdot\prod_{i=2}^{R}o_i^R$
	O, O, …, O	$\prod_{i=1}^{R}o_i^R\cdot p(\tilde{m}^R \mid m^R)$	0	…	0	$\prod_{i=1}^{R}o_i^R\cdot p(\tilde{m}^R \mid m^R)$	$\prod_{i=1}^{R}o_i^R$
	Total	$1-\tilde{o}^1$	0	…	0	$\tilde{o}^1$	1

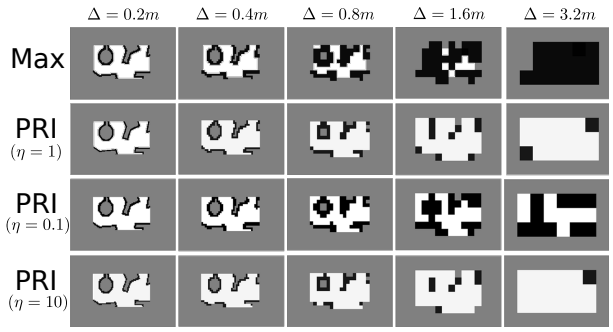

Fig. 4: A small map compressed using four different strategies. As cell edge length Δ grows, the PRI strategy retains map geometry for longer than maximum occupancy compression.

where the last case applies in the limit as $\lambda \to 1^+$.

The PRI solution gives us a simple compression rule: if the product of cell occupancy likelihoods in a given region is greater than 1, set the occupancy of the cell corresponding to that region in the compressed OG to 1. Likewise set the value to 0 if the product of likelihoods is less than 1, and to 0.5 if the product of likelihoods is 1.

While the optimal PRI solution yields reasonable compressed maps, Eq. (9) lends equal weight to free and occupied cells when calculating the occupancy value of a cell in the compressed map. For any application that heavily relies on raycasts, it is beneficial to ensure that rays that terminate on the original map also terminate on the compressed map. For these applications, one may introduce a heuristic to increase the fraction of occupied cells that are preserved through compression by multiplying the right-hand sides of the inequalities in Eq. (9) by $\eta \in (0, \infty)$. As $\eta \to 0^+$, occupied cells will be preserved through compression with higher frequency.

Denoting $\pi^R \equiv \prod_{i=1}^{R} \frac{o_i^R}{1-o_i^R}$ and applying this modification gives the $\sqrt{R}\times\sqrt{R} \to 1$ (or $\sqrt[3]{R}\times\sqrt[3]{R}\times\sqrt[3]{R} \to 1$ in 3D) compression function, f, for each region m^R:

$$\tilde{o}_*^1 = f(m^R, \eta) = \begin{cases} 0 & \text{if } \pi^R < \eta \wedge \pi^R \neq 1 \\ 1 & \text{if } \pi^R > \eta \wedge \pi^R \neq 1 \\ \frac{1}{2} & \text{otherwise} \end{cases}, \tag{10}$$

Figure 4 compares the PRI compression solution for different values of η against maximum occupancy compression (used by other OG compression algorithms such as OctoMap [9]). As the amount of compression increases, the PRI solution tends to retain major map features. Although changing the parameter η from a value of one causes the compression to deviate from the optimal PRI solution, it allows one to tune the likelihood that occupied cells are retained through compression.

B. Information Bottleneck Optimization

The PRI strategy in Sect. III-A determines a compression given a desired OG resolution. However, Fig. 2 suggests that one should also reduce the resolution of the OG as much as possible to increase computational efficiency of exploration. In this section we formulate a second optimization based on the Information Bottleneck (IB) method [19] that chooses a grid resolution minimizing both the redundancy between m^K and $C_n(m^K)$, and loss of mutual information with respect to a sensor measurement z.

IB is a widely used technique in signal processing for finding the optimal reduced representation $\hat{X}$ of a random variable X that preserves maximum information about a second random variable Y:

$$\min_{\hat{X}} \mathrm{I}(X;\hat{X}) - \beta \mathrm{I}(\hat{X};Y). \tag{11}$$

IB resembles PRI, but considers the effects of compression on the information between two data sets, as opposed to one. Similar to λ in the PRI optimization, β is a design parameter that trades compression for conservation of information. As $\beta \to 0$, the optimization tends towards the trivial lossy compression $\{\hat{X}\} = 0$, whereas when $\beta \to \infty$, $\hat{X}$ approaches its original representation X [15]. The two terms in the argument of Eq. (11) can equivalently be thought of as the information loss incurred by describing $\hat{X}$ with Y instead of with X [8].

Most importantly for OG compression, when combined with the PRI approach in Section III-A, the IB method can be used to find an optimal compression n^*:

$$n^* = \underset{n\in\mathbb{N}_0}{\operatorname{argmin}} \; \mathrm{I}_{\mathrm{CS}}\left(m^K; C_n(m^K)\right) - \beta \mathrm{I}_{\mathrm{CS}}\left(C_n(m^K); z\right). \tag{12}$$

The second term can be computed using Eq. (2), and is $2^{1\times n}$ times more efficient than computing Eq. (2) with respect to the uncompressed map m^K (where $d = 1$ because $\mathrm{I}_{\mathrm{CS}}(m; z_\tau)$ is computed using 1D raycasts). The first term, $\mathrm{I}_{\mathrm{CS}}(m^K; C_n(m^K))$, describes the divergence between the distributions $p(m^K, C_n(m^K))$ and $p(m^K)p(C_n(m^K))$, and

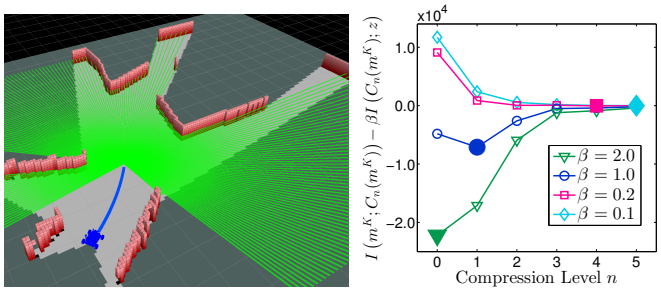

(a) (b)

Fig. 5: Uncompressed map and measurement taken from a planned future position (5a). With this map and expected laser scan, the compression level optimizing Eq. (12) (filled markers) decreases as β increases, favoring preservation of mutual information between the map and measurement as opposed to compression (5b).

can be computed by substituting these for $p(x_i)$ and $p(\hat{x}_i)$ in the definition of Cauchy-Schwarz divergence (Eq. (5)), using Table I to look up values for individual elements of the joint and marginal distributions during summation.

The joint distribution $p(m^R, \tilde{m}^R)$ in Table I can be computed by factoring it as $p(m^R)p(\tilde{m}^R \,|\, m^R)$. Since the variable $\tilde{m}^R$ is a deterministic piecewise function, f, of m^R and η (Eq. (10)), each element of the conditional distribution $p(\tilde{m}^R \,|\, m^R)$ is equal to 0 or 1. For a given pair of maps, M_1^R and M_2^R, assumed by the random variables m^R and $\tilde{m}^R$, the conditional distribution evaluates to 1 if compressing M_1^R yields the map M_2^R, and evaluates to 0 otherwise:

$$p(\tilde{m}^R = M_2^R \,|\, m^R = M_1^R) = \begin{cases} 1 & \text{if } p(\tilde{m}^R = M_2^R) = f(M_1^R, \eta) \\ 0 & \text{if } p(\tilde{m}^R = M_2^R) \neq f(M_1^R, \eta) \end{cases}. \tag{13}$$

Figure 5 displays the influence of β on the IB optimization for a multi-beam measurement captured from a planned future location. The optimization favors no compression when β is large, and maximum compression when β is small.

C. Adapting Occupancy Grid Compression Online

Rather than fixing the OG resolution when the map is initialized, we employ an adaptive strategy that recomputes a desired grid resolution with Eq. (12) online whenever the map has changed significantly. This approach allows the planner to re-evaluate the information trade-off whenever the complexity of the local map is altered. Using this adaptive method and propagating the efficiency gains from OG compression through to planning frequency and vehicle velocity make the robot slow down in complex regions, where the IB method prefers small values of n. Likewise, the vehicle will increase its velocity in open areas.

To trigger a new optimization, we monitor the mean entropy of cells in the robot's local map (in a bounding box around the robot and its planned paths). Whenever the difference between the current and previous mean cell entropies passes a threshold δ_{H}, we compute a set of compressed OGs $C_n(m^{\text{local}})$, $n = \{0, \ldots, n_{max}\}$, and evaluate Eq. (12) using these OGs and the current measurement.

$$\left| \mathbb{E}\left[\mathrm{H}_2(m^{\text{previous}})\right] - \mathbb{E}\left[\mathrm{H}_2(m^{\text{local}})\right] \right| \geq \delta_{\mathrm{H}}. \tag{14}$$

Calculating $\mathrm{H}_2(m^{\text{local}})$ has a fixed computational cost when the local map has a fixed size, as is the case using the planning strategy described in Sect. IV.

IV. Receding Horizon Planner

To move to informative regions in the environment, we generate sets of candidate actions by building a tree from a dictionary of motion primitives. Motion primitives densely sample the local workspace, allowing the robot to evaluate reward in places that frontier-based algorithms [20] might not consider. Additionally, motion primitives allow for high-speed maneuvering since they are generated by forward-simulating the robot's achievable dynamics.

Each motion primitive in the dictionary is computed by moving along an arc with a fixed linear and angular velocity [13]. After generating the dictionary, we build a tree of primitives to sample more locations. This is accomplished by rotating and translating the dictionary to a point a distance along the highest-reward path from the previous planning iteration, and repeating this process iteratively for the end-points of all primitives until a specified depth is reached.

The planner updates on a fixed frequency that is specified at run-time and recalibrated when the criteria in Eq. (14) is met. The planning configuration space is calculated with respect to the uncompressed map, and primitives that fall outside of the configuration space are pruned.

CSQMI is computed along each path (depth-first traversals of the primitive tree) every 5 m. To ensure that laser scans from sequential measurements on the path are independent (a requirement of z_τ in Eq. (2) [4]), we cache a grid of collision likelihoods between raycasts, and query it for every 5 m evaluation.

V. Results

To examine the effects of PRI OG compression and IB optimization on the accuracy and efficiency of information-based exploration, we performed experiments in simulation and on a 2D ground robot. In both sets of experiments, we assume that the vehicle is able to estimate its own state from IMU and laser measurements, and produce an accurate OG map of its surroundings in real-time. For state estimation and mapping we use a laser- and inertial-based SLAM implementation similar to the system described by Shen et al. [16], which leverages ICP for laser odometry [14], a histogram filter for localization, and an unscented Kalman filter (UKF) to fuse state estimates [18]. We assume no encoder odometry. The OG is updated at 10 Hz and has a 0.1 m uncompressed resolution. The robot's laser scanner sweeps in a 270° arc with 1081 beams, and has a max range of 30 m. Laser scans generally contain approximately 100 independent beams that are used to calculate Eq. (2).

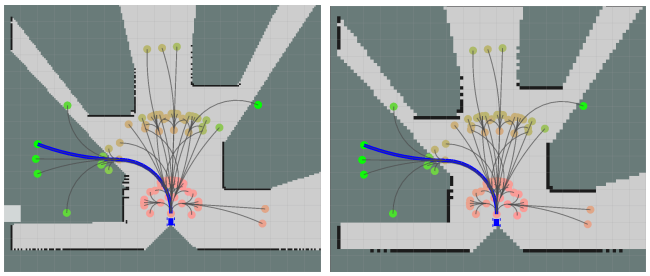

(a) $m^K, \Delta = 0.1$ m (b) $C_1(m^K), \Delta = 0.2$ m

(c) $C_3(m^K), \Delta = 0.8$ m (d) $C_5(m^K), \Delta = 3.2$ m

Fig. 6: CSQMI reward along motion primitives computed on compressed OGs. The best exploration path (blue), corresponding to the path maximizing Eq. (1), is only altered when $n = 5$. Green corresponds to high CSQMI reward, and red to low.

For parameters, we choose to deviate from the optimal PRI compression, instead using $\eta = 0.1$ in Eq. (10) to preserve walls through compression because computation of CSQMI is heavily affected by ray length. We choose $\beta = 0.5$ to persuade larger map compressions, and $\delta_{\text{H}} = 0.05$ in Eq. (14). These values were both chosen based on the environment's size; in general $\beta \in [0.2, 1.0]$ and $\delta_{\text{H}} \in [0.05, 0.1]$ work well for indoor environments. In most environments, compressing a 0.1 m resolution OG to cells with greater than 3.2 m resolution ($n > 5$) yields a mostly-free or mostly-occupied compressed OG. $n = 5$ is therefore set as an upper limit. The primitive dictionary is generated with $v \in [0.3, 9.0]$ m/s, $\omega \in [\pm\pi/4]$ rad/s, and with a depth of 3. These parameters result in a dictionary containing 729 primitives. Some primitives are pruned before computing CSQMI due to obstacle collisions in the full-resolution map.

CSQMI rewards computed with Eq. (2) are shown at the endpoints of paths in the primitive tree for maps compressed with PRI to different resolutions in Fig. 6. The path optimizing Eq. (1) on the uncompressed map is still chosen until $n = 3$, which allows CSQMI reward to be computed $2^3 = 8$ times as efficiently.

A. Simulation Experiments

Simulated exploration trials on a maze-like 25×25 m map were conducted to examine the effects of OG compression on the robot's path. During each map update, the robot's local map was compressed to a fixed resolution ($n \in \{0, 2, 4\}$) using Eq. (10), and the compressed OG was used to calculate CSQMI rewards (Eq. (2)). Resulting exploration paths are shown in Fig. 7. Without applying the techniques introduced in Sect. III-A, the vehicle is only able to safely move at

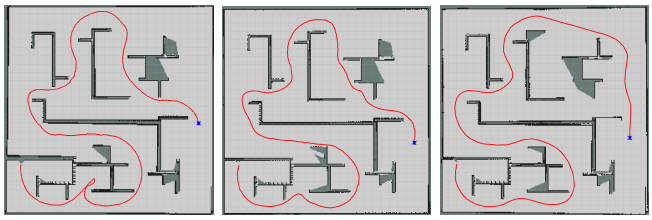

(a) m^K
$\Delta = 0.1$ m
$\dot{\mathbf{x}} = 0.35$ m/s

(b) $C_2(m^K)$
$\Delta = 0.4$ m
$\dot{\mathbf{x}} = 1.50$ m/s

(c) $C_4(m^K)$
$\Delta = 1.6$ m
$\dot{\mathbf{x}} = 3.00$ m/s

Fig. 7: Varying n causes the robot to navigate slightly further from walls. Due to exponential increases to planning frequency, the vehicle is able to increase its maximum velocity from 0.35 m/s to 3.0 m/s (Table II). The explored map m^K is shown in each figure to visualize map completeness.

TABLE II: Simulated exploration trial data (Fig. 7).

n	Δ (m)	Planning Freq. (Hz)	Maximum Velocity (m/s)	Time (s)
0	0.1	1.5	0.35	230.0
2	0.4	6.0	1.5	54.7
4	1.6	24.0	3.0	31.9

0.35 m/s, due to computational constraints enforcing 1.5 Hz maximum planning frequency. After compressing to $n = 4$, the vehicle's velocity is no longer limited by planning frequency, but by the modeled maximum angular velocity. As n increases, paths close to walls become occupied in the compressed map (for small η) and yield low CSQMI reward, so the robot chooses paths in the middle of free space with a higher frequency. Table II shows planning frequency, velocity, and total trial time for these simulations.

B. Ground Robot Experiments

To test the adaptive strategy introduced in Sect. III-C, we explored a 35×35 m section of Carnegie Mellon University's Field Robotics Center with a ground robot. The ground robot was equipped with a MicroStrain 3DM-GX3-35 IMU, a Hokuyo URG-30LX 30 m range laser scanner, and an onboard computer with an Intel Core i5 processor and 8 GB RAM. The robot's motor controllers and wheels limit its maximum forward velocity to 1.6 m/s.

Figure 8 depicts the ground robot, its 72 m exploration path through the environment (beginning from the bottom), and the adapted compression level and UKF velocity estimate. Dashed lines in Fig. 8c correspond to times when the adaptation condition in Eq. (14) is met. Colored dashed lines mark times when Eq. (14) is met and Eq. (12) computes a new value for n. Since the planner generates primitives in the robot's forward direction, entropy is generally computed in the local map in front of the robot. n remains at 4 in most of the free regions in the trial, and reduces to 0, 1, and 2 in locations where compression results in large reductions to CSQMI reward (e.g. the first $n = 0$ region occurs as the robot moves through a doorway). Planning frequency is modified as n changes, and the vehicle accelerates or decelerates accordingly.

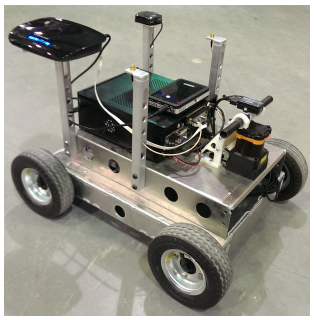

(a) Robot platform

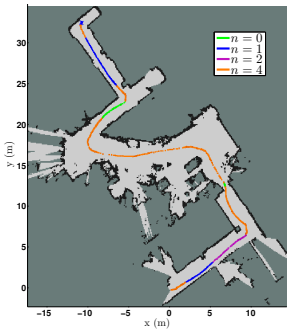

(b) Exploration path

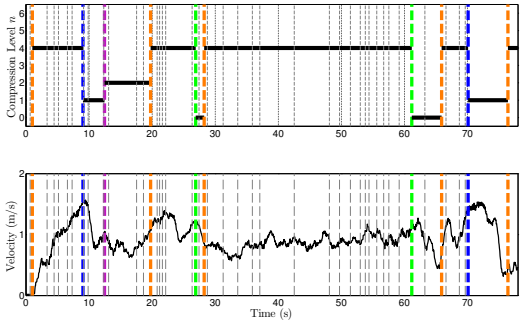

(c) Time evolution of n and velocity.

Fig. 8: As the ground robot explores, it recomputes an OG resolution and adapts its planning horizon accordingly.

VI. Summary and Future Work

We developed information-theoretic optimizations to reduce the computational expense of evaluating information-based reward for autonomous exploration. In doing so, we formulated a lossy compression strategy for OGs using the Principle of Relevant Information. The solution to this formulation is a simple compression rule that retains map structure well compared to maximum occupancy compression. To account for distortions to information-based reward computed using sensor measurements, we introduced a method of choosing an OG resolution using the Information Bottleneck method. By adaptively performing these optimizations online, the robot chooses an OG resolution based on the local environment. These results were validated through simulation and ground robot experiments, where robots were tasked with exploring previously unknown areas. The presented methods increase the computational efficiency of evaluating information-theoretic reward, enabling high-speed exploration through cluttered 2D indoor environments. In the future, we plan to apply these results to 3D OGs in the aerial domain, where larger numbers of actions are required to explore a space.

References

[1] F. Amigoni and V. Caglioti. An information-based exploration strategy for environment mapping with mobile robots. *Robot. Auton. Systs.*, 58(5):684–699, 2010.

[2] F. Bourgault, A. A. Makarenko, S. B. Williams, B. Grocholsky, and H. F. Durrant-Whyte. Information based adaptive robotic exploration. In *Proc. IEEE/RSJ Intl. Conf. on Intelli. Robots and Systs.*, volume 1, pages 540–545, Lausanne, Switzerland, 2002.

[3] W. Burgard, M. Moors, D. Fox, R. Simmons, and S. Thrun. Collaborative multi-robot exploration. In *Proc. IEEE Intl. Conf. on Robotics and Autom.*, volume 1, pages 476–481, Takamatsu, Japan, 2000.

[4] B. Charrow, S. Liu, V. Kumar, and N. Michael. Information-theoretic mapping using cauchy-schwarz quadratic mutual information. In *Proc. IEEE Intl. Conf. on Robotics and Autom.*, Seattle, USA, 2015.

[5] E. Einhorn, C. Schroter, and H. Gross. Finding the adequate resolution for grid mapping-cell sizes locally adapting on-the-fly. In *Proc. IEEE Intl. Conf. on Robotics and Autom.*, pages 1843–1848, Shanghai, China, 2011.

[6] A. Elfes. *Occupancy grids: a probabilistic framework for robot perception and navigation*. PhD thesis, Carnegie Mellon University, 1989.

[7] H. J. S. Feder, J. J. Leonard, and C. M. Smith. Adaptive mobile robot navigation and mapping. *Intl. J. Robotics Res.*, 18(7):650–668, 1999.

[8] B. C. Geiger, C. Feldbauer, and G. Kubin. Information loss in static nonlinearities. In *Proc. IEEE Intl. Sym. on Wireless Commun. Systs.*, pages 799–803, Aachen, Germany, 2011.

[9] A. Hornung, K. M. Wurm, M. Bennewitz, C. Stachniss, and W. Burgard. OctoMap: An Efficient Probabilistic 3D Mapping Framework Based on Octrees. *Auton. Robots*, 34(3):189–206, 2013.

[10] J. J. Im, A. Leonessa, and A. Kurdila. A real-time data compression and occupancy grid map generation for ground-based 3d lidar data using wavelets. In *Proc. ASME Dynamic Systs. and Control Conf.*, Cambridge, USA, 2010.

[11] B. J. Julian, S. Karaman, and D. Rus. On mutual information-based control of range sensing robots for mapping applications. In *Proc. IEEE/RSJ Intl. Conf. on Intelli. Robots and Systs.*, pages 5156–5163, Tokyo, Japan, 2013.

[12] H. Kretzschmar and C. Stachniss. Information-theoretic compression of pose graphs for laser-based slam. *Intl. J. Robotics Res.*, 31(11):1219–1230, 2012.

[13] M. Pivtoraiko, I. A. Nesnas, and A. Kelly. Autonomous robot navigation using advanced motion primitives. In *Proc. IEEE Aerospace Conf.*, pages 1–7, Big Sky, USA, 2009.

[14] F. Pomerleau, F. Colas, R. Siegwart, and S. Magnenat. Comparing icp variants on real-world data sets. *Auton. Robots*, 34 (3):133–148, 2013.

[15] J. C. Principe. *Information theoretic learning: Rényi's entropy and kernel perspectives*. Springer Science & Business Media, 2010.

[16] S. Shen, N. Michael, and V. Kumar. Autonomous multi-floor indoor navigation with a computationally constrained mav. In *Proc. IEEE Intl. Conf. on Robotics and Autom.*, pages 20–25, Hong Kong, China, 2011.

[17] C. J. Taylor and D. Kriegman. Exploration strategies for mobile robots. In *Proc. IEEE Intl. Conf. on Robotics and Autom.*, pages 248–253, Atlanta, USA, 1993.

[18] S. Thrun, W. Burgard, and D. Fox. *Probabilistic robotics*. MIT press, 2005.

[19] N. Tishby, F. C. Pereira, and W. Bialek. The information bottleneck method. *arXiv preprint physics/0004057*, 2000.

[20] B. Yamauchi. A frontier-based approach for autonomous exploration. In *Proc. IEEE Sym. on Comput. Intelli. in Robot. and Autom.*, pages 146–151, Monterey, USA, 1997.